Real-Space Imaging of Thomson Charge Configurations in Superfluid Helium Nanodroplets

Thomas Pohl,[1] Jan Mayerhofer,[1] Hanqing Liu,[2] Arin Mizouri,[3] Hao Sha,[2] Masoomeh Mahmoodi Darian,[1] Fabio Zappa,[1] Andrew M. Ellis,[2] David J. Wales,[4] Shengfu Yang,[2,*] and Paul Scheier[1,†]

[1]Department of Ion Physics and Applied Physics, University of Innsbruck, 6020 Innsbruck, Austria
[2]School of Chemical, Earth and Environmental Sciences, University of Leicester, Leicester LE1 7RH, UK
[3]Department of Physics, Durham University, Durham DH1 3LE, UK
[4]Yusuf Hamied Department of Chemistry, University of Cambridge, Cambridge CB2 1EW, UK

ABSTRACT.
Predicting the lowest-energy arrangement of like charges on a sphere defines the Thomson problem, a long-standing challenge with analytical solutions only for a few small systems. We report a real-space experimental realization using superfluid helium nanodroplets, where surface-localized charges are tagged by singly charged gold nanoparticles and recorded as transmission electron microscopy imprints. The observed configurations reveal Thomson charge ordering from finite-*N* minima to curvature-frustrated Coulomb crystallization, establishing helium nanodroplets as a directly imageable platform for charge organization on spherical surfaces.

I. INTRODUCTION.

In 1904, when J. J. Thomson developed a model of the atom, he was searching for the ground state of a system of N identical charges that repel each other and are located on the surface of a sphere [1]. Although it is not a useful model for atomic structure, the Thomson problem has since found diverse applications in systems with spherical topologies, including spherical viruses [2], fullerenes [3], crystallography [4], colloidal shells [5] and colloidosomes [6], cell envelopes of archaebacteria [7], coding theory [8], and geography [9]. The common feature is that defects must be present to permit packing on a spherical surface. On a local scale, charges arrange on a triangular lattice, and each charge has six nearest neighbors. However, Euler's theorem requires the existence of at least 12 pentagonal disclinations [10], corresponding to charges with five nearest neighbors. Lower-energy packings can be achieved in larger systems via additional defects that reduce strain energy, including dislocations [11-14] and grain boundary scars [10, 15, 16], which can involve combinations of pentagons and heptagons. Recently, Amore [17] numerically solved the Thomson problem on a spherical cap.

The most favorable packing is often the principal focus of interest, which defines a global optimization problem. Since the number of local minima is expected to grow exponentially with N [18, 19] the search rapidly becomes more difficult, although the long-ranged Coulomb potential supports fewer local minima than typical interatomic potentials [20]. For $N \leq 100$, the global minima obtained in different calculations are in good agreement [13, 21-24], and putative global minima have been reported for N up to a few thousand [25].

In 1998, Steve Smale included the Thomson problem in his list of eighteen unsolved mathematical problems for the 21st century [26], where it appears as problem #7, "Distribution of Points on the 2D-Sphere". To date, analytical solutions exist only for small systems [27, 28]. Multiply charged clusters and droplets have been considered experimental model systems for the Thomson problem. However, in most classical droplets, such as water, the charges are not confined to the surface but instead distribute throughout the droplet volume [29]. In contrast, charge centers in superfluid helium are highly mobile [30, 31] and are expected to localize close to the surface. Recent computational studies based on time-dependent helium density functional theory showed that ionic impurities, such as Na^+ and Ca^+, preferentially reside close to the helium nanodroplet (HND) surface at equilibrium, supporting the use of HNDs as a platform for experimental realization of the Thomson charge configurations [32].

Laimer et al. [33] demonstrated that HNDs can stabilize very high charge states, establishing them as promising model systems for studying charge ordering under well-defined conditions. Utilizing coherent diffraction imaging of heavily Xe-doped multiply-charged HNDs, Feinberg et al. observed that most of the Xe is located in the form of charged clusters close to the surface [34]. The reconstructed structures agree qualitatively with numerical solutions of the Thomson problem; however, the spatial resolution of the retrieved images in this study does not allow for a quantitative comparison. Experiments that combine surface confinement, weak screening, and single-

*Contact author: sfy1@leicester.ac.uk
†Contact author: paul.scheier@uibk.ac.at

particle real-space readout have therefore remained unavailable.

Here, we present a novel approach to capture orthographic projections of experimental realizations of the Thomson problem, using superfluid HNDs as a nearly spherical, weakly screening, ultra-cold environment in which surface-localized charges can reorganize with minimal external perturbation. In contrast to three-dimensional Coulomb crystals formed in ion traps [35, 36], this approach provides a particularly well-defined route to charge ordering on a sphere. The charge configurations are tagged by singly charged gold nanoparticles (Au-NPs) containing a few hundred atoms, transferred onto a transmission electron microscopy (TEM) grid upon droplet impact, and subsequently imaged by TEM. For droplets containing up to $N = 36$ charge carriers, the experimentally observed structures closely reproduce the geometries corresponding to the global minima predicted by previous numerical solutions.

II. METHODS

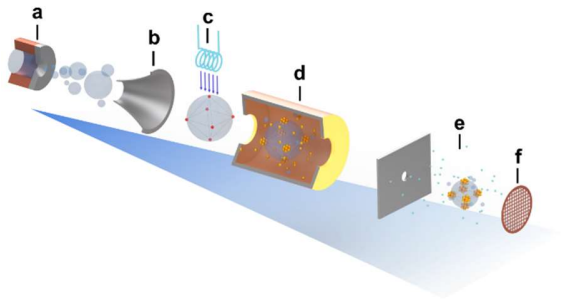


Fig. 1: Schematic of the experimental setup. (a) Pinhole nozzle for supersonic expansion of precooled Helium gas into vacuum. (b) Conical skimmer selecting the central HND-beam portion. (c) Nier-type electron impact source. (d) Resistively-heated crucible containing Au-vapor. (e) Shrinking of HNDs via collisions with room temperature helium gas. (f) TEM-grid to deposit the Au-NPs.

Fig.1 shows schematically the experimental procedure. A technical rendering of the setup as well as details of the experimental methods and data analysis can be found in the Supplemental Material (SM) [37]. In brief, HNDs were produced by continuous expansion of precooled helium gas (99.9999% purity) into vacuum through a pinhole nozzle of 5 µm diameter at a stagnation pressure of 20 bar and a nozzle temperature of 5.75 K. The central portion of the expanding free jet was selected by a conical skimmer with a 0.5 mm diameter orifice positioned 5 cm downstream of the nozzle. The droplet beam was crossed with an electron beam in a Nier-type ion-source operated at an electron energy of 35 eV and a current of 150 µA, resulting in the formation of multiple positive charge carriers. For droplets larger than 1 µm the electron current was increased to 200 µA to better visualize the structural motifs. Atoms are picked up from gold vapor formed in a resistively heated crucible (~1500 K). Neutral gold atoms entering the droplets are rapidly thermalized and drawn towards the surface-localized charge centers via ion-induced-dipole interaction. Charge transfer to the first-arriving gold atom and subsequent aggregation of additional dopants result in the formation of singly charged Au-NPs near the pre-existing charge centers. The average nanoparticle size is determined by the number of dopant atoms captured per droplet, divided by its charge state. The substantial binding energy released during particle growth is dissipated by evaporation of helium atoms from the surrounding superfluid matrix. The cross-sections for electron ionization and dopant pickup have the same droplet size dependence, i.e., proportional to the square of the HND diameter. Consequently, the nanoparticle size does not depend on the diameter of the HNDs and can be tuned via electron energy, current, and oven power [38]. In the present experiments, Au-NPs containing approximately 700 atoms were produced to ensure reliable identification of individual particles across all imprints by TEM.

To suppress the large number of small droplets inherent to the exponential size distribution generated under the present expansion conditions [39] and ensure well-separated nanoparticle imprints, the doped HND beam was passed through a buffer-gas region before deposition. Room-temperature helium at a pressure of $\sim 5.9 \times 10^{-2}$ Pa induces collisional evaporation, leading to an approximately size-independent reduction of the droplet diameter, as discussed in the SM [37]. As a result, small droplets are fully evaporated, whereas larger ones survive the passage. Buffer-gas filtering explains, why $N = 5$ is the smallest Thomson configuration that we were able to observe. It modifies the observed droplet-size distribution but does not change the angular arrangement of charges which is governed primarily by Coulomb ordering on the droplet surface.

The doped helium nanodroplets were deposited onto TEM grids, producing two-dimensional nanoparticle imprints upon impact. Rapid evaporation of the helium matrix leaves the gold nanoparticles immobilized on the substrate. Deposition was performed over short exposure times (< 1 s) by rotating the sample holder in and out of the beam to minimize imprint overlap for subsequent imaging and structural analysis.

III. RESULTS and DISCUSSION

*Contact author: sfy1@leicester.ac.uk

†Contact author: paul.scheier@uibk.ac.at

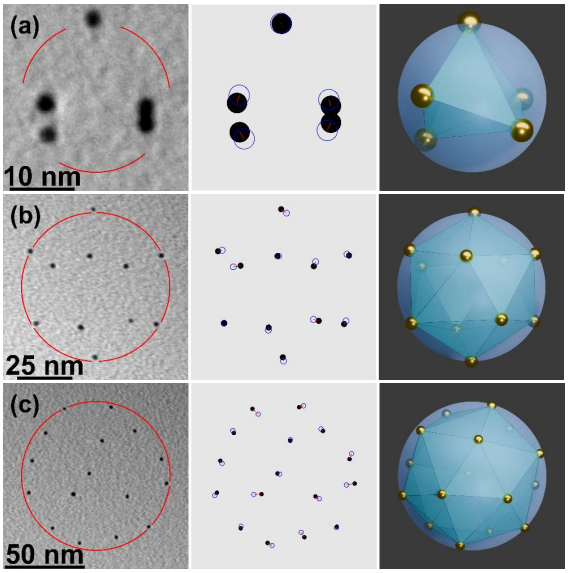


Fig. 2: Experimental imprints and projected Thomson configurations for small charged helium nanodroplets. TEM images of imprints containing $N = 5$, 11, and 16 singly charged Au-NPs are shown from top to bottom. The left column shows the TEM image of each imprint, with the reconstructed droplet boundary indicated by a red circle. The middle column compares the experimentally determined nanoparticle centroids (black dots) with the best-fitting orthographic projection of the corresponding ideal Thomson configuration (open blue circles). The right panel displays a three-dimensional rendering of the same Thomson configuration.

A total of 25 well-separated imprints of superfluid helium nanodroplets containing $N = 5$–36 singly charged Au-NPs per droplet were analyzed. The underlying three-dimensional arrangements were inferred by comparing each imprint with the corresponding global minima for N-point Thomson configurations reported in previous work [12, 24]. The theoretical structures were rotated, orthographically projected onto the imaging plane, and rescaled to optimize agreement with the experimental patterns (see SM [37]). For droplets with a radius up to about 175 nm ($\leq$ 36 Au-NPs), the procedure converges reliably, revealing a clear correlation between the observed two-dimensional imprints and the projected three-dimensional ideal Thomson configurations (Fig. 2(a–c)). In this regime, the fitted arrangements are consistent with the orthographic projections of the corresponding low-N Thomson global minima, including highly symmetric polyhedral motifs.

For larger systems, corresponding to particle numbers exceeding approximately $N = 40$, both experimental and theoretical factors complicate a definitive assignment of specific Thomson geometries. On the theoretical side, the rapidly increasing number of local minima in the Thomson potential energy landscape makes trapping of the charges in low-lying local minima increasingly likely, rather than relaxation to the global minimum [18, 24]. The long-range Coulomb potential is expected to produce funneled landscapes [40], which have been visualized for selected sizes in previous work [41], but for larger N, multiple funnels are likely to arise. Experimentally, larger imprints are more susceptible to overlapping projected nanoparticles and contamination by incidental particles originating from other droplets, thereby introducing additional ambiguities in the extracted configurations. These sporadic outliers are difficult to exclude from the two-dimensional imprints reliably. Improved suppression of overlap and incidental particles should therefore make it possible to probe competing low-energy morphologies associated with different funnels in the Thomson landscape. The observed agreement with the reported global minima for smaller N suggests that relaxation is efficient in these systems. When alternative low-energy structures exist, we would expect them to correspond to local funnels, and a well-defined distribution of locally optimal geometries may become accessible.

While full fitting of ideal Thomson configurations becomes unreliable at intermediate imprint sizes ($r >$ 175 nm), the largest imprints observed here (400–900 nm) exhibit a distinct and highly reproducible structural pattern, as exemplified in Fig. 3. Most prominently, the central region of the imprints displays a clear hexagonal lattice punctuated by isolated fivefold disclinations. This defect structure is characteristic of spherical crystallography in the large-N limit and arises from the frustration of hexagonal packing on a curved surface [10, 16, 18, 24]

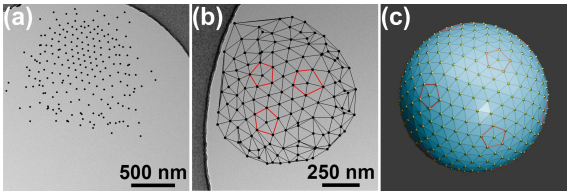


Fig. 3: Local hexagonal order and topological defects in large-droplet imprints. (a), TEM imprint of a large helium droplet with a radius of about 1 µm. Extracted particle positions are overlaid as enlarged black dots. The particle density decreases toward the imprint periphery, resulting in a washed-out outer region. (b) Hemispherical experimental imprint in the range of $375 < r < 600$ nm. Neighboring particles are connected via triangulated edges to visualize the local hexagonal order. Red pentagons mark fivefold disclinations. (c)

*Contact author: sfy1@leicester.ac.uk
†Contact author: paul.scheier@uibk.ac.at

Rendering of an ideal Thomson configuration with 400 singly charged Au-NPs, shown as an orthographic projection of the visible hemisphere.

The emergence of this motif suggests that the central region of large imprints corresponds to a largely undistorted orthographic projection of Au-NPs originally located on the hemisphere of the droplet facing the TEM grid upon deposition. The absence of particles originating from the opposite hemisphere is consistent with previous reports that helium nanodroplets colliding with a solid surface undergo splashing that leads to partial backscattering of a substantial fraction of charged dopants [42]. Ions with a mass up to a few thousand Dalton (Da) were ejected from helium nanodroplets with an average diameter well below 50 nm [43]. The complete and distortion-free imprints of Au-NPs, with an average mass of ~140 kDa assuming spherical geometry, in helium droplets with $r < 175$ nm observed in the present study indicate that splashing depends on both the dopant mass and droplet size.

The interpretation of an orthographic projection of the visible nanoparticles located on the hemisphere facing the TEM-grid upon deposition is supported by comparison with an ideal large-N Thomson configuration. Fig. 3c shows a render of 400 singly charged Au-NPs in the global Thomson minimum [24]. The simulated configuration of the visible nanoparticles located on the hemisphere facing the observer reproduces the characteristic structural features observed experimentally in the central region of large imprints. The clear emergence of this motif provides experimental evidence that large helium nanodroplet imprints retain structural signatures expected for Coulomb ordering on a curved surface.

Towards the periphery of the largest observed imprints with radii exceeding 600 nm (Fig. 3a), the overall particle density decreases, as qualitatively expected for particles that are pushed off-center with the spreading liquid. In contrast, for a smaller HND (Fig. 3b) in the range of $375 < r < 600$ nm the increase in particle density towards the imprint boundary agrees with an orthographic projection of particles homogeneously dispersed on the surface of a sphere. At the same time, the increasingly perturbed pattern suggests contributions from Au-NPs originating from the upper hemisphere of the droplet at the moment of deposition. The pronounced angular variation in peripheral particle density further indicates that dynamical perturbations of the droplet topology during impact also contribute to distortions of the observed particle geometry in the large-droplet limit.

For small HNDs, where all nanoparticles are deposited, the particle density decreases with increasing droplet size (see Fig. 2 and the Figs. S5 and S6 in the SM [37]). This disagrees with a constant surface charge density of differently sized HNDs passing through an electron beam with roughly the same velocity.

The reduction of HND size upon gold pickup, nanoparticle growth, and passage through helium gas, was estimated using kinetic gas theory, the surface collision rate, and the cohesive energy per atom of gold clusters [44] (see SM [37]). This approach yields a size-independent radius reduction of ~75 nm under the present experimental conditions. Correcting the measured imprint radii by this value enables determination of the initial HND size and surface charge density before gold pickup (solid symbols in Fig. S4). For the present experimental conditions, we obtain a constant surface charge density $\sigma = 63.1 \pm 1.9$ e/μm^2 (horizontal line in Fig. S4), as expected for differently sized HNDs passing with roughly the same velocity through an electron beam.

V. CONCLUSIONS

We have developed an experimental platform to investigate real-space configurations associated with the global optimization problem posed by J.J. Thomson in 1904. In this approach, multiply charged superfluid helium nanodroplets serve as nearly spherical, weakly screening hosts, while surface-localized charge centers are tagged by singly charged Au-NPs and captured as TEM imprints after deposition. For droplets containing up to 36 Au-NPs, the observed two-dimensional imprints are consistent with orthographic projection of the corresponding three-dimensional global minima of Thomson configurations, suggesting effective relaxation to the most favorable structure consistent with the funneled energy landscape expected from calculations [41]. Larger imprints show local hexagonal order interrupted by fivefold disclinations, indicating the onset of curvature-frustrated crystallization in the large-N limit. Currently, incomplete deposition as well as spreading of nanoparticles towards the rim of the imprints is limiting our ability to compare imprints of large HNDs with computed solutions of the Thomson problem or to assign slightly aspherical droplet shapes. We expect that displacement of nanoparticles, as well as backscattering of nanoparticles, can be reduced by lowering the speed of impinging droplets below the Landau critical velocity. With such improved control over deposition, overlap suppression, and large-droplet reconstruction, this platform should enable experimental studies of competing low-energy

*Contact author: sfy1@leicester.ac.uk
†Contact author: paul.scheier@uibk.ac.at

Thomson configurations at substantially larger charge numbers. Since rotating helium nanodroplets can adopt aspherical shapes [45], the same approach may also provide access to charge ordering on more complex curved surfaces.

ACKNOWLEDGMENTS

Financial Support was provided by the Austrian Science Fund, FWF via the project Grant-DOI 10.55776/P34563, Land Tirol, Grant: SupremeBy-Nano, and by the UK Engineering and Physical Science Research Council (EPSRC, Grant code: EP/V027255/1), the Leverhulme Trust (Grant codes: RPG-2020-152 and RPG-2024-116).

DATA AVAILABILITY

Custom MATLAB code used for nanoparticle segmentation, clustering, and Thomson-configuration fitting is available at Zenodo [DOI: 10.5281/zenodo.18386136], together with example input data and instructions to reproduce the analysis shown in Fig. 2 and Figs. S5 and S6 in the SM [37].

[1] J.J. Thomson, Philos. Mag., 7, 237-265 (1904).
[2] M.A. Kanso, J.H. Piette, J.A. Hanna, and A.J. Giacomin, Phys. Fluids, 32, 113101 (2020).
[3] H.W. Kroto, J.R. Heath, S.C. Obrien, R.F. Curl, and R.E. Smalley, Nature, 318, 162-163 (1985).
[4] W.T.M. Irvine, V. Vitelli, and P.M. Chaikin, Nature, 468, 947-951 (2010).
[5] V.N. Manoharan, M.T. Elsesser, and D.J. Pine, Science, 301, 483-487 (2003).
[6] A.D. Dinsmore, M.F. Hsu, M.G. Nikolaides, M. Marquez, A.R. Bausch, and D.A. Weitz, Science, 298, 1006-1009 (2002).
[7] U.B. Sleytr, and D. Pum, Q. Rev. Biophys., 58, e4 (2025).
[8] N.J.A. Sloane, Sci. Am., 250, 116-125 (1984).
[9] R. Barnes, Int. J. Digit. Earth, 13, 803-816 (2020).
[10] M. Bowick, A. Cacciuto, D.R. Nelson, and A. Travesset, Phys. Rev. Lett., 89, 185502 (2002).
[11] A. Pérez-Garrido, and M.A. Moore, Phys. Rev. B, 60, 15628-15631 (1999).
[12] E.L. Altschuler, and A. Pérez-Garrido, Phys Rev E, 73, 036108 (2006).
[13] D.J. Wales, H. McKay, and E.L. Altschuler, Phys. Rev. B, 79, 224115 (2009).
[14] A. Pérez-Garrido, Phys. Rev. B, 62, 6979-6981 (2000).
[15] M.J. Bowick, A. Cacciuto, D.R. Nelson, and A. Travesset, Phys. Rev. B, 73, 024115 (2006).
[16] A.R. Bausch, M.J. Bowick, A. Cacciuto, A.D. Dinsmore, M.F. Hsu, D.R. Nelson, M.G. Nikolaides, A. Travesset, and D.A. Weitz, Science, 299, 1716-1718 (2003).
[17] P. Amore, Physica A:Statistical Mechanics and Its Applications, 682, 131140 (2026).
[18] T. Erber, and G.M. Hockney, Phys. Rev. Lett., 74, 1482-1482 (1995).
[19] F.H. Stillinger, and T.A. Weber, Science, 225, 983-989 (1984).
[20] D.J. Wales, Energy Landscapes, Cambridge University Press2004.
[21] E.L. Altschuler, T.J. Williams, E.R. Ratner, F. Dowla, and F. Wooten, Phys. Rev. Lett., 72, 2671-2674 (1994).
[22] E.L. Altschuler, T.J. Williams, E.R. Ratner, R. Tipton, R. Stong, F. Dowla, and F. Wooten, Phys. Rev. Lett., 78, 2681-2685 (1997).
[23] Y. Xiang, D.Y. Sun, W. Fan, and X.G. Gong, Phys. Lett. A, 233, 216-220 (1997).
[24] D.J. Wales, and S. Ulker, Phys. Rev. B, 74, 212101 (2006).
[25] X.J. Lai, J.K. Hao, R.B. Xiao, and Z.H. Fu, Expert Syst. Appl., 238, 121704 (2024).
[26] S. Smale, Math. Intell., 20, 7-15 (1998).
[27] R.E. Schwartz, Exp. Math., 22, 157-186 (2013).
[28] R.E. Schwartz, Constr. Approx., 51, 537-564 (2020).
[29] V. Kwan, A. Malevanets, and S. Consta, J. Phys. Chem. A, 123, 9298-9310 (2019).
[30] L. Skrbek, J. Low Temp. Phys., 212, 232-250 (2023).
[31] F. Reif, and L. Meyer, Phys. Rev., 119, 1164-1173 (1960).
[32] E. García-Alfonso, F. Ancilotto, M. Barranco, F. Cargnoni, N. Halberstadt, and M.R. Pi, J. Chem. Phys., 161, 224303 (2024).
[33] F. Laimer, L. Kranabetter, L. Tiefenthaler, S. Albertini, F. Zappa, A.M. Ellis, M. Gatchell, and P. Scheier, Phys. Rev. Lett., 123, 165301 (2019).
[34] A.J. Feinberg et al., Phys. Rev. Res., 4, L022063 (2022).
[35] S. Willitsch, M.T. Bell, A.D. Gingell, S.R. Procter, and T.P. Softley, Phys. Rev. Lett., 100, 043203 (2008).
[36] M. Drewsen, C. Brodersen, L. Hornekaer, J.S. Hangst, and J.P. Schiffer, Phys. Rev. Lett., 81, 2878-2881 (1998).
[37] See Supplemental Material for DOI for additional figures, methodological details, which includes Refs. [46-51].

*Contact author: sfy1@leicester.ac.uk
†Contact author: paul.scheier@uibk.ac.at

[38] S. Kollotzek, O.V. Lushchikova, L. Tiefenthaler, F. Zappa, and P. Scheier, Int. J. Mol. Sci., 23, 3613 (2022).
[39] J.P. Toennies, and A.F. Vilesov, Angew. Chem. Int. Edit., 43, 2622-2648 (2004).
[40] D.J. Wales, Science, 293, 2067-2070 (2001).
[41] D. Mehta, J.X. Chen, D.Z. Chen, H. Kusumaatmaja, and D.J. Wales, Phys. Rev. Lett., 117, 028301 (2016).
[42] P. Martini, S. Albertini, F. Laimer, M. Meyer, M. Gatchell, O. Echt, F. Zappa, and P. Scheier, Phys. Rev. Lett., 127, 263401 (2021).
[43] M. Kappe, A. Schiller, E. Gruber, D. Jank, M. Gatt, G. Schöpfer, M. Oncák, A.M. Ellis, and P. Scheier, J. Chem. Phys., 159, 204302 (2023).
[44] O.D. Häberlen, S.C. Chung, M. Stener, and N. Rösch, J. Chem. Phys., 106, 5189-5201 (1997).
[45] S.M.O. O'Connell et al., Phys. Rev. Lett., 124, 215301 (2020).
[46] M. Wang, G. Audi, A.H. Wapstra, F.G. Kondev, M. MacCormick, X. Xu, and B. Pfeiffer, Chinese Physics C, 36, 1603-2014 (2012).
[47] R.J. Donnelly, and C.F. Barenghi, J. Phys. Chem. Ref. Data, 27, 1217-1274 (1998).
[48] C.B. Alcock, V.P. Itkin, and M.K. Horrigan, Can. Metall. Q., 23, 309-313 (1984).
[49] C. Kittel, Introduction to Solid State Physics, 8th ed., John Wiley & Sons, Inc, Hoboken, NJ, 2005.
[50] J.R. Rumble, CRC Handbook of Chemistry and Physics, 106 ed., CRC Press, Boca Raton, FL, 2025.
[51] F. Laimer, F. Zappa, and P. Scheier, J. Phys. Chem. A, 125, 7662–7669 (2021).

*Contact author: sfy1@leicester.ac.uk
†Contact author: paul.scheier@uibk.ac.at